ACS NANO

www.acsnano.org

ARTICLE

Close-Packed Ices in Nanopores

Kenji Mochizuki,* Yuji Adachi, and Kenichiro Koga*

Cite This: *ACS Nano* 2024, 18, 347−354

Read Online

ACCESS | Metrics & More | Article Recommendations | Supporting Information

ABSTRACT: **Water molecules in any of the ice polymorphs organize themselves into a perfect four-coordinated hydrogen-bond network at the expense of dense packing. Even at high pressures, there seems to be no way to reconcile the ice rules with the close packing. Here, we report several close-packed ice phases in carbon nanotubes obtained from molecular dynamics simulations of two different water models. Typically they are in plastic states at high temperatures and are transformed into the hydrogen-ordered ice, keeping their close-packed structures at lower temperatures. The close-packed structures of water molecules in carbon nanotubes are identified with those of spheres in a cylinder. We present design principles of hydrogen-ordered, close-packed structures of ice in nanotubes, which suggest many possible dense ice forms with or without nonzero polarization. In fact, some of the simulated ices are found to exhibit ferroelectric ordering upon cooling.**

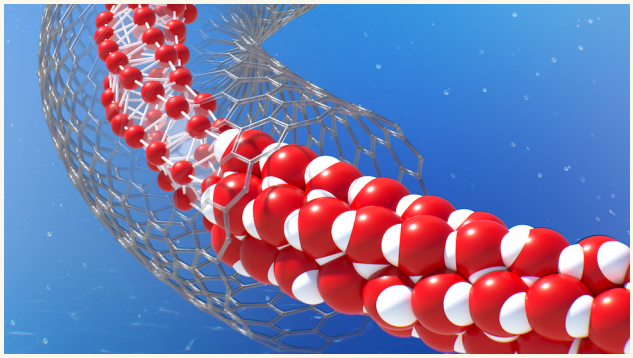

KEYWORDS: *Close-packed ices, Ice nanotubes, Carbon nanotubes, Continuous freezing, Ferroelectric ices*

INTRODUCTION

Water demonstrates a persistent ability to form four-coordinated hydrogen bond networks as it freezes into one of crystalline solids under varying conditions.[1] Eighteen out of the 20 ice polymorphs confirmed by experiment to date (those with Roman numerals attributed to their names) satisfy the ice rules: every molecule is hydrogen-bonded to its four neighbors, thus forming a perfect four-coordinated network.[2−5] (Ices X and XVIII are the exceptions as they are no longer a molecular solid consisting of discrete H_2O molecules.) Water is very flexible in transforming into different ices with different densities, ranging from the low-density hexagonal and cubic ices (Ih and Ic) to the high-density ices with the body-centered cubic (bcc) and body-centered tetragonal lattices (VII and VIII). However, no ice form has been found so far which has a close-packed arrangement of oxygen atoms, i.e., face-centered cubic (fcc) or hexagonal close-packed (hcp) lattice. This implies that the formation of a four-coordinated hydrogen-bond network and the closest packing of water molecules are incompatible with each other, and water always chooses the former even at pressures as high as tens of GPa.

Formation of four-coordinated hydrogen bond networks in solid water is not limited to bulk environments. A variety of nano-ice forms in confined geometries have been predicted by simulation[6−11] and confirmed by experiment.[12−15] Despite the fact that the nano-ices bear no similarity in structure to bulk ices, they have perfect or nearly perfect hydrogen bond networks. Examples are quasi-one-dimensional ices formed in carbon nanotubes.[8,10−12] Among those ices the single-walled ice nanotubes[8,12] have crystalline or helical structures built by rolling up a sheet of square hydrogen-bond net with water molecules at its vertices. Water molecules in ice nanotubes satisfy the ice rules, but the structures identified thus far are not close packing in cylindrical geometries.

Here we report the results of molecular dynamics (MD) simulations of water confined in carbon nanotubes, demonstrating the coexistence of four-coordinated perfect network formation and close packing. The close-packed arrangements of water molecules in such situations are those found for argon atoms in nanotubes[16] but at the same time each molecule is hydrogen-bonded to its four neighbors. We also show that the ices with close-packed structure transform into *plastic* ices, in which molecules rotate more or less freely. The plastic ices of confined water have not been reported so far, and they are different in structure from those which have been found for bulk water by simulation.[17−19] The transformations between plastic and crystalline ices are found to be either continuous or discontinuous, depending upon the diameter of carbon

Received: July 30, 2023
Revised: December 5, 2023
Accepted: December 12, 2023
Published: December 18, 2023

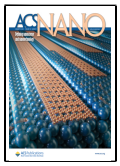

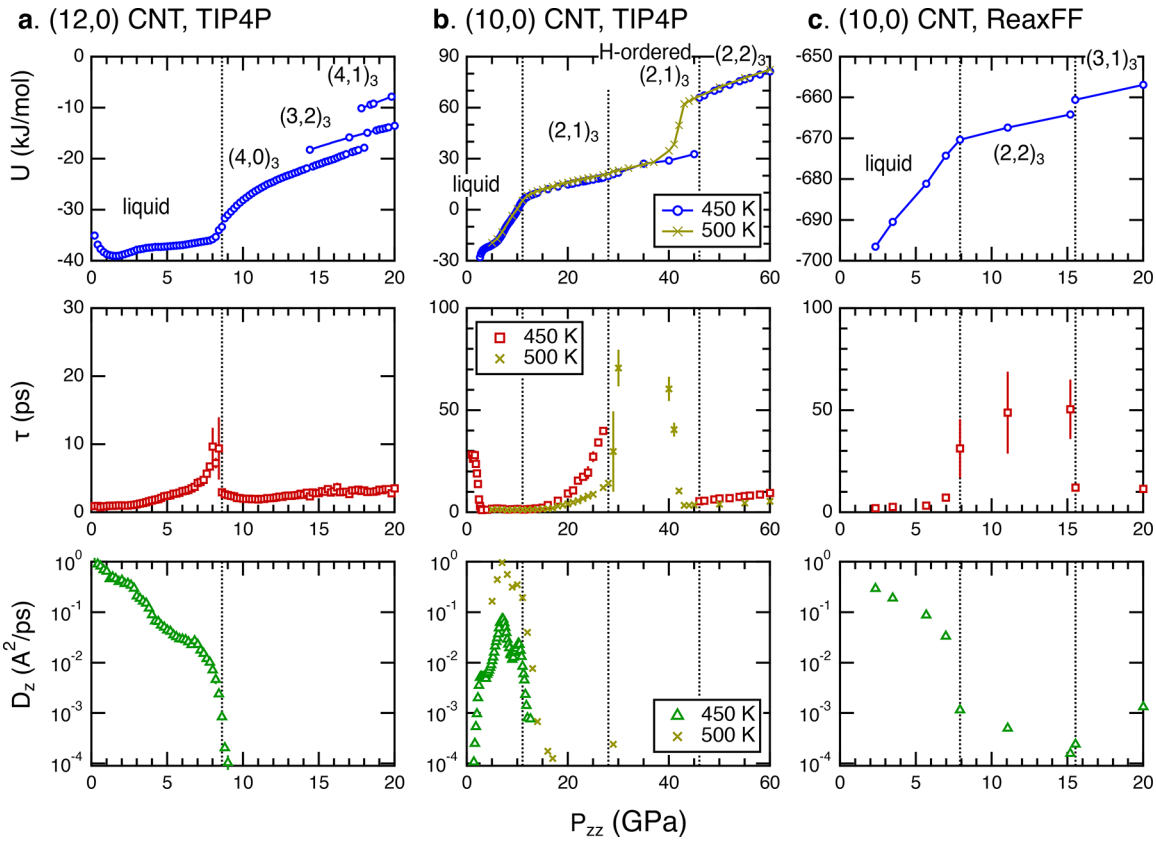

Figure 1. Isothermal transformation from liquid to close-packed ice nanotubes. The potential energy (U, top), the relaxation time of the autocorrelation function (τ, middle), and the diffusion coefficient along the axial direction (D_z, bottom) are plotted as a function of the axial pressure (P_{zz}) for water in (a) the (12,0) carbon nanotube (CNT) at 500 K and (b) the (10,0) carbon nanotube at 450 and 500 K, both using the TIP4P model, and (c) the (10,0) carbon nanotube at 500 K using the ReaxFF model. The dashed black lines indicate the P_{zz} to distinguish different water structures (based on 450 K for panel b). The hydrogen-ordered close-packed ice nanotube is denoted as "H-ordered".

nanotubes and the temperature during isothermal compression.

RESULTS AND DISCUSSION

We performed MD simulations of two different model systems: one is the TIP4P water,[20] a common rigid-body model, confined in a smooth-wall potential,[8] and the other is a fully atomistic system described by the reactive force field ReaxFF.[21] Phase behavior, structure, and dynamics of confined water were examined for each model system as functions of the axial pressure P_{zz} (the pressure tensor element along the tube axis) at a fixed temperature and as functions of the temperature T at a fixed axial pressure.

Figure 1 shows the total potential energy U, the relaxation time τ of the dipole−dipole autocorrelation function for a water molecule, and the diffusion coefficient D_z of water along the tube axis, all as a function of P_{zz} at fixed temperature. The plots in Figure 1a are of TIP4P water in the (12,0) carbon nanotube at a fixed temperature of 500 K. Water is in a liquid state when P_{zz} is close to the ambient pressure as already known from the computed phase diagram of water in carbon nanotubes at atmospheric pressure.[11] The values of diffusion coefficient D_z and rotational relaxation time τ also confirm that neither translational nor rotational motions of molecules are hindered. It is also clear from snapshots of molecules that there is no long-range order in structure and no perfect hydrogen-bond network (Supporting Information (SI) Figure S1). As the pressure approaches 8.6 GPa, D_z decreases by 3 orders of magnitude and τ increases monotonically from 1 to 10 ps, indicating that confined water is becoming glassy. The orientational relaxation time τ decreases abruptly at P_{zz} = 8.6 GPa and remains less than 4 ps as the pressure increases further. At the same pressure, 8.6 GPa, the D_z curve exhibits a kink and the value of D_z becomes too small to be measured before P_{zz} exceeds 10 GPa. Therefore, one may conclude that water is in the solid state at least above 10 GPa. With increasing pressure in the range P_{zz} > 8.6 GPa, the potential energy U jumps to higher values twice. In a reverse change of pressure, U discontinuously drops to lower values at different pressures, exhibiting hysteresis. This implies that there exist three distinct solid phases, and we will confirm them below.

The structure of single-walled ice nanotubes reported so far can be represented by a roll-up vector on a square-lattice sheet,[11] just as the structure of carbon nanotubes is defined by a roll-up vector (n, m) on a hexagonal graphite lattice. Figure 2a, for example, displays the $(3, 1)_4$ ice nanotube in the (12, 0) carbon nanotube, the stable ice form at 0.1 GPa and 200 K. Note the subscript "4" attached to (3, 1) denoting the square-lattice sheet. The single-walled ice nanotubes whose structure is defined by the roll-up vector $(n, m)_4$ have a perfect hydrogen bond network, because the structure is topologically equivalent to the square net. We report here ice nanotubes that are not represented by roll-up vectors $(n, m)_4$. They exist at higher pressures and higher temperatures. At 500 K and at P_{zz} = 8.6

https://doi.org/10.1021/acsnano.3c07084
ACS Nano 2024, 18, 347−354

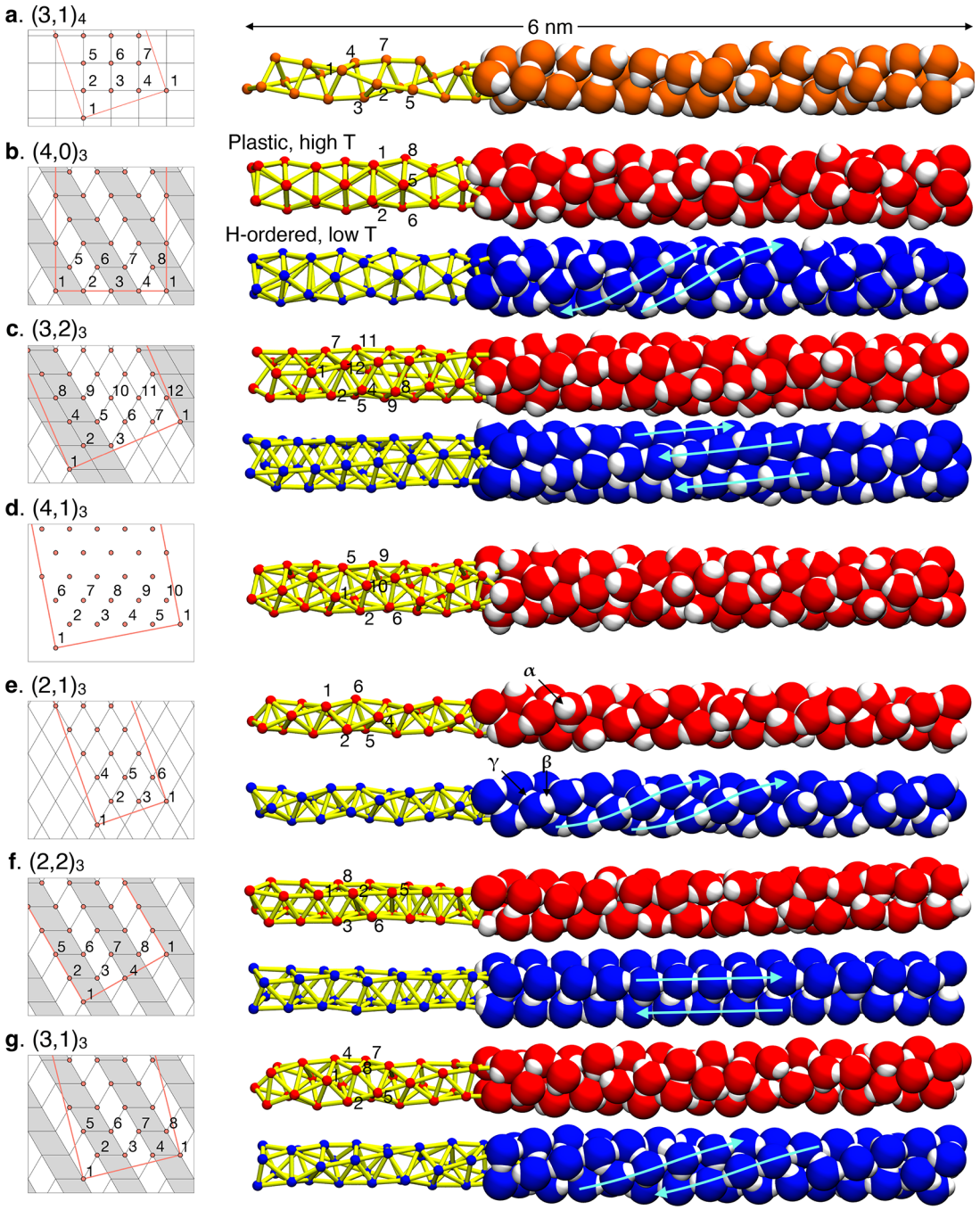

Figure 2. Molecular structures of (a) the already-reported $(3,1)_4$ ice nanotube and (b–g) the discovered close-packed ice nanotubes with roll-up vectors of $(4, 0)_3$, $(3, 2)_3$, $(4, 1)_3$, $(2, 1)_3$, $(2, 2)_3$, and $(3, 1)_3$. The left panel shows the schematic projection on the square- or triangle-lattice sheet, including the water molecules (pink circles) and the hydrogen bonds (black lines) for the hydrogen-ordered form. Each ice nanotube is made by rolling up the rectangular area bordered in pink. On the right, the side view (6 nm in total) is represented by the framework (left, small balls and yellow lines) and the van der Waals spheres of water molecules (right). The numbering on the yellow framework corresponds to that on the lattice sheet. The molecular structures with red (top) and blue (bottom) spheres, respectively, represent plastic ice nanotubes and the corresponding hydrogen-ordered forms. The sky blue arrows indicate the "flow" of hydrogen bonds. The structures in panels a–e are obtained by using the TIP4P model, while those in panels f and g are obtained by the reaxFF model. The labels of α, β, and γ in panel e show the typical hydrogen orientations discussed in Figure 4c.

GPa and above, there appears an unfamiliar ordered ice form with an arrangement of oxygen atoms (or centers of mass of water molecules) which can be expressed by the roll-up vector $(4, 0)_3$ on the triangle–lattice sheet, the subscript "3" denoting the triangle net. The ice structure along with the triangle net is depicted in Figure 2b. As P_{zz} increases further toward 20 GPa, two more different ice forms are found in accord with the stepwise changes in U (Figure 1a top). The ice structures are again expressed by roll-up vectors on the triangle lattice, namely, $(3, 2)_3$ and $(4, 1)_3$ (see Figure 2c,d). These structures made by rolling up the triangle-lattice sheet are close packing of spheres in cylindrical pores.[22−24] The ice nanotubes represented by the vectors $(4, 0)_3$, $(3, 2)_3$, and $(4, 1)_3$

https://doi.org/10.1021/acsnano.3c07084
ACS Nano 2024, 18, 347−354

described above correspond to phases VII, VIII, and IX of spheres closely packed in cylindrical pores.[23]

Confined water at high pressures of $P_{zz} \geq 10$ GPa and at 500 K is in a solid state (Figure 1a, bottom). However, the rotational relaxation time τ (Figure 1a, middle) indicates that water molecules rotate even more freely than they do in liquid states at pressures of just below 8.6 GPa. Therefore, ice nanotubes $[(4, 0)_3]$, $[(3, 2)_3]$, and $[(4, 1)_3]$ may be classified as plastic solids. The existence of plastic phases in bulk water has been predicted by computer simulations with a variety of water models.[17−19,25−31] As we will see below, plastic ice forms are ubiquitous in cylindrical pores with varying diameters.

Figure 1b shows the results at a fixed temperature of 450 K for TIP4P water in the (10, 0) carbon nanotube. As the pressure increases, liquid water transforms continuously into ice nanotube, at around 11 GPa, whose structure is characterized by the vector $(2, 1)_3$ (Figure 2e), and upon increasing pressure further the $(2, 1)_3$ ice nanotube transforms discontinuously into the $(2, 2)_3$ ice nanotube at around 46 GPa (Figure 2f). Water molecules in the $(2, 1)_3$ ice nanotube rotate more or less freely at lower pressures around 11 GPa (τ is as small as that for liquid water), and therefore the $(2, 1)_3$ ice nanotube in the pressure range is plastic ice. The molecular rotation is gradually suppressed with increasing pressure and practically frozen in the range of $28 < P_{zz} < 45$ GPa as τ exceeds 200 ps in that range. At 46 GPa and above, one finds the $(2, 2)_3$ ice nanotube in which water molecules rotate again freely (see Figure 1b, middle).

We shall examine how the rotational motions of water molecules in the $(2, 1)_3$ ice nanotube freeze at around 28 GPa. Structural analysis indicates that the gradual increase in τ (and hence the loss of the plastic behavior) is accompanied by the growth of a hydrogen-bond network. There is no discontinuity in U at that pressure but the slope dU/dP_{zz} increases discontinuously. The resulting hydrogen-bond network is essentially perfect and ordered. The bottom panel of Figure 2e shows the hydrogen-ordered $(2, 1)_3$ ice nanotube observed at pressures between 28 and 45 GPa. One can see that it has a double helix structure of hydrogen-bonded water molecules. The double helices are interconnected with hydrogen bonds, which also form a single helix, and hence, every water molecule has four hydrogen-bonded neighbors. The double helices have the same directions of OH···OH···OH··· with ··· meaning hydrogen bonds (sky-blue arrows in the figure). This form of ice nanotube has a notable feature that is not shared with any bulk ice: the coexistence of close packing and observance of the ice rules. As shown later, there are more examples of the fully hydrogen-bonded, close-packed structures that have not been reported.

Simulation results obtained along the 500 K isotherm are depicted in Figure 1b. The transformation pressure from the liquid to the $(2, 1)_3$ plastic ice nanotube is nearly the same as that along the 450 K isotherm. The overall reduction in τ from that at 450 K is observed at pressures ranging from 10 to 30 GPa (see the middle panel in Figure 1b), a characteristic manifestation of the temperature effect on molecular rotation in the plastic ice. Transformation of the plastic ice nanotube to the hydrogen-ordered ice nanotube takes place at a pressure approximately 3 GPa higher than that at 450 K. According to the potential energy and τ, the subsequent phase transition to the $(2,2)_3$ ice nanotube occurs at a pressure approximately 5 GPa lower. This means that at each phase boundary the entropy of the hydrogen-ordered $(2, 1)_3$ ice nanotube is smaller than the plastic ice nanotube of either the $(2, 1)_3$ or $(2, 2)_3$ structure. The potential energy changes with pressure (the upper panel in Figure 1b) indicate that the transition from the hydrogen-ordered $(2, 1)_3$ ice nanotube to the plastic $(2, 2)_3$ ice nanotube occurs discontinuously at 450 K but continuously at 500 K. This indicates that the first-order-like phase boundary between the hydrogen-ordered $(2, 1)_3$ and plastic $(2, 2)_3$ ice nanotubes disappears at some point in the domains of $450 \text{ K} \leq T \leq 500$ K and $40 \text{ GPa} \leq P_{zz} \leq 45$ GPa. Such a point may be identified as the "critical" point, another example of terminals of liquid−solid or solid−solid phase boundaries found in quasi-one-dimensional substances in nanopores.

MD simulations of water in carbon nanotubes using the ReaxFF also give phase behaviors similar to what we found for the TIP4P water. Figure 1c shows the results for water in the (10, 0) carbon nanotube at 500 K. With increasing pressure, liquid water gradually transforms into the $(2, 2)_3$ plastic ice nanotube at around 7.9 GPa, followed by a discontinuous structure transformation to the $(3, 1)_3$ plastic ice nanotube at 15.5 GPa. The respective molecular structures are shown in Figure 2f,g. The ice phases observed are different from those of the TIP4P water in the (10, 0) carbon nanotube (Figure 1b) because the effective tube diameters are different for the two model systems: it is larger in the ReaxFF model (SI Figure S2), and qualitatively, the same phase behaviors are obtained for the two model systems if the effective tube diameters are close to each other (SI Figure S3).

The six plastic ice nanotubes reported above are all represented by the roll-up vectors $(m, n)_3$ on the triangle-lattice sheet unlike ice nanotubes at ambient conditions whose structure is described by $(m, n)_4$ on the square net. This means that water molecules under pressures greater than 10 GPa and at temperatures higher than 400 K arrange themselves to achieve close packing like equal spheres in cylinders.[16,22,24] Note that increasing the axial pressure P_{zz} has the same effect as increasing the pore diameter because both particles and the confining wall are soft; accordingly, the order of appearance of different ice nanotubes with increasing pressure $[(2, 1)_3 \rightarrow (2, 2)_3 \rightarrow (3, 1)_3$ in the (10, 0) carbon nanotube and $(4, 0)_3 \rightarrow (3, 2)_3 \rightarrow (4, 1)_3$ in the (12, 0) carbon nanotube] is consistent with the order of close-packed structures of argon particles with increasing tube diameter $[(2, 1)_3 \rightarrow (3, 0)_3 \rightarrow (2, 2)_3 \rightarrow (3, 1)_3 \rightarrow (4, 0)_3 \rightarrow (3, 2)_3 \rightarrow (4, 1)_3]$,[16] except that there is no ice nanotube with the $(3, 0)_3$ structure. The reasons, both kinetic and thermodynamic, behind the absence of the $(3, 0)_3$ ice phase still need elucidation. Here we note one possibility. In the phase diagram of argon in a smooth cylindrical nanotube, the $(3, 0)_3$ phase occupies a narrower diameter range compared to its adjacent phases, $(2, 1)_3$ and $(2, 2)_3$.[16] It is possible that the anisotropy in pair potentials of water could raise the free energy of the $(3, 0)_3$ phase over that of $(2, 1)_3$ or $(2, 2)_3$ and make the former phase metastable.

The plastic ice nanotubes have close-packed structures, whereas the ice nanotubes satisfying the ice rules have less dense structures. There is another class of ice nanotubes in which close packing and observance of ice rules coexist. We already observed one example: the $(2, 1)_3$ plastic ice nanotube transforms into a hydrogen-ordered ice nanotube with the same arrangement of oxygen atoms at pressures above 28 GPa. Figure 2e shows its structure and hydrogen-bond network. Likewise, five plastic ice nanotubes $[(2, 1)_3, (2, 2)_3, (3, 1)_3, (4, 0)_3$, and $(3, 2)_3]$ transform into the corresponding hydrogen-ordered close-packed ice nanotubes as the temperature is

https://doi.org/10.1021/acsnano.3c07084
ACS Nano 2024, 18, 347−354

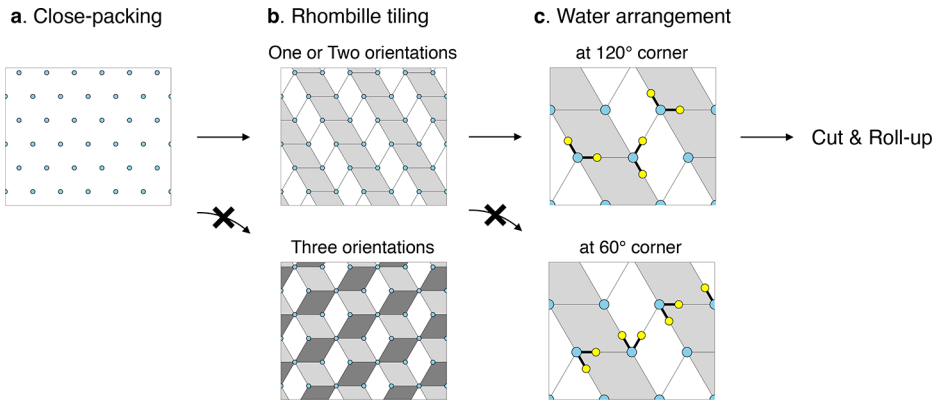

Figure 3. Design principle of the hydrogen-ordered close-packed ice nanotubes. Sky-blue and yellow circles, respectively, represent oxygen and hydrogen atoms. Gray lines represent hydrogen bonds.

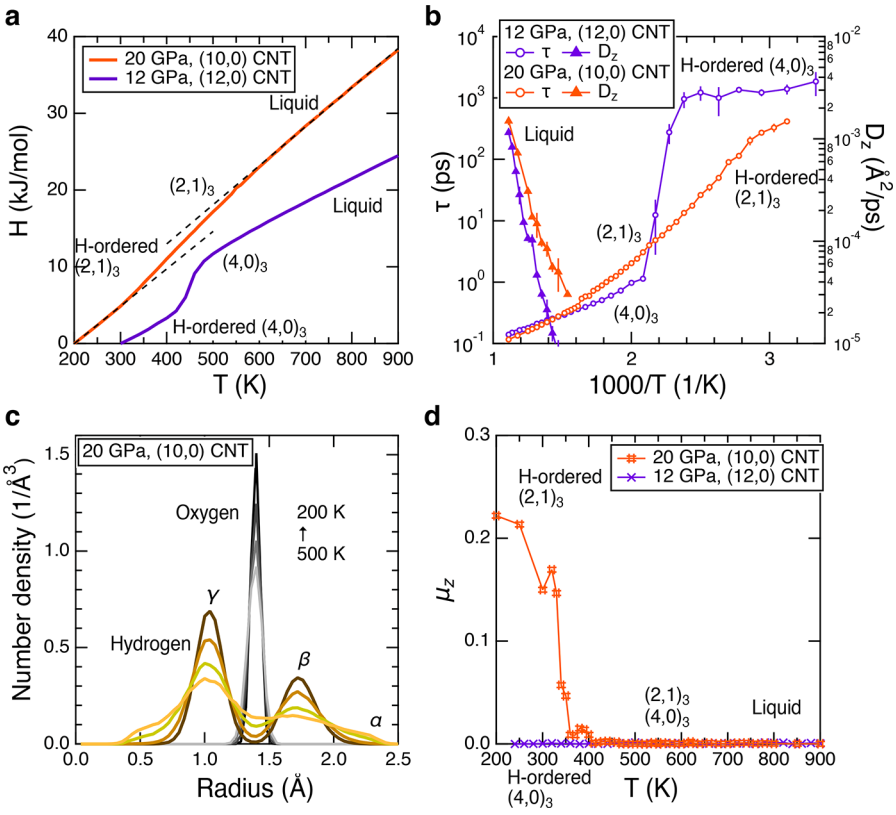

Figure 4. Isobaric transformation from liquid water to plastic to hydrogen-ordered close-packed ice nanotubes at 20 GPa in the (10,0) carbon nanotube and at 12 GPa in the (12,0) carbon nanotube (both using TIP4P water model): (a) Enthalpy H against temperature T (H is shifted to be zero at the respective lowest temperatures). The dashed linear lines are drawn as a guide. (b) τ and D_z against $1/T$. (c) Distributions of oxygen (gray) and hydrogen (orange) atoms as a function of the radial distance from the tube axis at temperatures of 200, 300, 400, and 500 K. The peaks labeled α, β, and γ correspond to three typical hydrogen orientations in Figure 2e. (d) z-axis component of the net polarization per molecule μ_z, when the water electric dipole moment is represented by a unit vector, against T.

decreased at a fixed pressure. Their molecular structures are shown in the right bottom panels in Figure 2b,c,e,f. The left panels in the same panels show a schematic description of the hydrogen-bond network (gray lines), in which each water molecule is surrounded by *six* neighbors but satisfies the ice rules forming hydrogen bonds with *four* of them. None of the bulk ices belong to this class; they satisfy the ice rules at the expense of close packing.

The Supporting Information Movie S1 provides an intuitive visualization of two distinct dynamic behaviors of the hydrogen-bond network. It compares the $(4, 0)_3$ plastic ice nanotube at 500 K to the corresponding hydrogen-ordered form at 240 K, both confined within the (12, 0) carbon nanotube at 12 GPa (see Figure 2b for snapshots). Notably, the movie reveals that water molecules in plastic ice nanotube exhibit incessant rotation while those in the hydrogen-ordered form remain relatively static.

Figure 3 outlines the design principle underlying the creation of hydrogen-ordered, close-packed ice nanotubes. First, oxygen atoms of water molecules were arranged to form the regular triangle lattice (Figure 3a). Second, identical 60° rhombi are tessellate on the lattice sheet so that the vertices

https://doi.org/10.1021/acsnano.3c07084
ACS Nano 2024, 18, 347−354

match the lattice sites (Figure 3b). The sides of rhombi represent hydrogen bonds. To satisfy the ice rules, there must be exactly four rays from each vertex. Tiling with one or two rhombus orientations meets the condition (e.g., the top in Figure 3b), but the tiling with three orientations violates the condition (the bottom in Figure 3b). Third, each water molecule should be oriented so that its two hydrogen atoms lie on two sides forming a 120° angle (the top in Figure 3c) but not on two sides forming a 60° angle (the bottom in Figure 3c). This is due to the geometrical restriction of the H−O−H bond angle. Finally, the sheet is cut into a rectangular shape and rolled up to create the tubular structure. This design principle enables the prediction of all possible single-walled ice nanotubes with a hydrogen-ordered close-packed arrangement. It should be noted that any combinations of light-gray and white stripes, which are different from those in Figure 2b,c,e,g, also satisfy the ice rules.

Figure 4a shows the isobaric change in enthalpy H ($\equiv U + pV$) of confined water (TIP4P) with temperature under two typical conditions: 12 GPa in the (12, 0) carbon nanotube and 20 GPa in the (10, 0) carbon nanotube, where the $(4, 0)_3$ and $(2, 1)_3$ plastic ice nanotubes are observed, respectively. Figure 4b displays the Arrhenius plots of τ and D_z under the same conditions. No discontinuous changes are observed for H and τ over the whole temperature range. However, the slopes dH/dT and $d\tau/d(1/T)$ change significantly when the plastic ice nanotubes are transformed to the corresponding hydrogen-ordered ice nanotubes. The change in dH/dT for the $(4, 0)_3$ ice nanotube at 460 K is sharp, while that for the $(2, 1)_3$ ice nanotube is more gradual over a wide temperature range from 500 to 350 K. The change in enthalpy for the $(4, 0)_3$ ice nanotube at 460 K predominantly arises from the change in potential energy (Figure S4). The transformation between plastic solid and liquid states is confirmed by finite values of D_z at and above 700 K (Figure 4b), but it is indiscernible in the temperature dependences of H and τ. As earlier studies demonstrated,[8,32] water confined in carbon nanotubes freezes into ice nanotubes either continuously or discontinuously, depending on the tube diameter, temperature, and pressure. The continuous structural changes are achieved via the microscopic segregation of ordered and disordered phases. Upon continuous freezing, structural and dynamical order parameters change at a maximum rate (with temperature or pressure) when crossing the Widom line, an extrapolation line of a solid−liquid coexistence curve beyond the critical point. For example, an abrupt change in H results in a bump in the isobaric heat capacity. Freezing of liquid water to the $(4, 0)_3$ plastic ice nanotube upon cooling along the isobar of 12 GPa is accomplished without any detectable change in dH/dT (see the violet curve in Figure 4a). By contrast, freezing to the same ice nanotube upon compression along the isotherm of 500 K can be identified by a variation in dH/dP_{zz}, although H still changes continuously at this stage (Figure 1a). Thus, further exploration of the temperature−pressure phase diagram may find the first-order phase transition from liquid to plastic ice nanotubes as well as a critical point between them.

We now examine how the average orientation of water molecules changes as the plastic $(2, 1)_3$ ice nanotube transforms into the hydrogen-ordered $(2, 1)_3$ ice nanotube. Figure 4c shows the density distribution of oxygen and hydrogen atoms as a function of the radial distance from the tube axis. The oxygen distribution functions at different temperatures have a single peak with the same peak position, indicating that the plastic and hydrogen-ordered ice nanotubes are both single-walled, and their diameters are essentially the same. In contrast, three distinct peaks can be seen for the hydrogen distribution, which are denoted by α, β, and γ. The hydrogen distribution is broad at higher temperatures (e.g., 500 K), indicating that water molecules in plastic states orient their OH covalent bonds even toward the carbon nanotube wall (α in Figure 4c). As the temperature decreases, the distribution is gradually localized to form two peaks (β and γ in Figure 4c). Representative orientations of water molecules corresponding to the three peaks, α, β, and γ, are indicated in Figure 2e. The continuous hydrogen ordering is consistent with the plots of H and τ in Figure 4a b.

Zeng et al. showed that some of the ice nanotubes can exhibit ferroelectric ordering: e.g., pentagonal and heptagonal ice nanotubes [$(5, 0)_4$ and $(7, 0)_4$] are ferroelectric as they have the odd number of rows of hydrogen-bonded molecules.[33] We find that some of the close-packed ice nanotubes can also be ferroelectric. When water gradually freezes into the $(2, 1)_3$ ice nanotube upon cooling at 20 GPa in the (10, 0) carbon nanotube, it exhibits spontaneous electric polarization. On the other hand, for example, no polarization is observed when water freezes into the $(4, 0)_3$ ice nanotube. Figure 4d shows the contrasting temperature dependences of the z-component of the net polarization per molecule, μ_z, when the unit vector is used to represent the water electric dipole moment. It is found that $\mu_z = 0.22$ for the $(2, 1)_3$ ice nanotube at 200 K, which corresponds to 0.72 e/nm^2 (12 μC/cm^2) using the electric dipole moment of the TIP4P model (0.45 e Å) and the effective inner diameter of the (10, 0) carbon nanotube (4.58 Å). It is clear that the hydrogen arrangement shown in Figure 2e gives a nonzero polarization unlike the one shown in Figure 2b. In the $(2, 1)_3$ ice nanotube, the two possible alignments along the opposite directions in the z-axis are identical with each other. One alignment persists for a certain period and the other takes it over, a typical length of the intervals being longer with decreasing temperature. The spontaneous polarization inversion suggests that an external electric field can determine the alignment direction. If μ_z is averaged over an infinitely long time or is obtained for an infinitely long ice nanotube, its value would be zero at any finite temperature because the single ice nanotube is basically a one-dimensional system. However, ice nanotubes with finite lengths or those in a bundle of carbon nanotubes may have nonzero net polarization at finite temperatures.

In our simulations, close-packed ice nanotubes are found to be stable, at least, in the pressure range from 8 to 60 GPa and at temperatures below 500 K. Experimental verification of our predicted ice forms is not impossible at lower pressures in that range using a diamond anvil cell since it was demonstrated that water-filled single-walled carbon nanotubes are stable up to 17 GPa.[34] Experimental observation of the phase behavior and ice structures at ultrahigh pressures would be challenging. As confirmed by recent experimental studies of bulk ice,[3,35] there is a possibility that the quantum effect on proton dynamics is significant beyond some pressure, say, 50 GPa, and in that case classical simulation methods would be invalid.

CONCLUSION

In conclusion, MD simulations using both the rigid and reactive models of water revealed the phase behavior of water in carbon nanotubes, in which water molecules spontaneously form unfamiliar close-packed structures at high pressures. The

https://doi.org/10.1021/acsnano.3c07084
ACS Nano 2024, 18, 347−354

close-packed ices are either plastic or hydrogen-ordered ones; the arrangements of oxygen atoms are identical to those for close packing of spheres in a cylinder, and they are constructed by rolling up a triangle-lattice sheet. We found four helical and one straight hydrogen-ordered close-packed ice forms, all of which satisfy the ice rules. To the best of our knowledge, close-packed ice forms satisfying the ice rules have not been reported for bulk or confined water while plastic close-packed (fcc) bulk ice[18] and hexagonal-close-packed bilayer ice,[36,37] both violating the ice rules, have been predicted by simulations. Our simulation results strongly suggest that the close-packed ice forms exist at high-pressure regions in the phase diagram of water in cylindrical pores. Determination of the phase boundaries of those ices and examination of critical points associated with those boundaries are important subjects of future work. A more complete picture of the phase diagram of water in well-defined nanopores would help us to understand the behaviors and roles of water in minerals, porous materials, and biological systems.

METHODS

Rigid-Body Water Model. MD simulations for the rigid-body water model of TIP4P[20] in a smooth cylindrical tube, which represents a single-walled carbon nanotube, are carried out, in the same manner as in our previous studies.[8,11,32] A periodic boundary condition is applied in the axial direction (z-axis). There is no substance present around the carbon nanotube along the x- and y-axes. The eligibility of this set of force fields in predicting ice structures in carbon nanotubes and melting temperatures has been confirmed experimentally.[38] The temperature T and the internal axial pressure P_{zz} (the pressure tensor parallel to the z-axis) are controlled using the modified Nosé−Andersen's method. Trajectories are generated by the Gear predictor−corrector method with a time step of 0.5 fs. The examined (10, 0) and (12, 0) single-walled carbon nanotubes have diameters of 7.975 and 9.523 Å, respectively. The effective inner diameter, which is used to compute the volume contribution to the enthalpy, is defined by subtracting the diameter of a carbon atom (3.4 Å) from these diameters.

The number of water molecules is 200. For each condition, an equilibration MD simulation in the isothermal−isobaric ensemble ($NP_{zz}T$) is carried out for more than 100 ps, using the temperature correction, followed by a subsequent production $NP_{zz}T$-MD simulation for more than 400 ns.

Reactive Water Model. MD simulations with the ReaxFF reactive force fields[21] are carried out for water molecules in the atomistic (10, 0) single-walled carbon nanotube, using the LAMMPS package (17 November 2016 version).[39] Water molecules are represented by the water2010 model[40] and parameters for the water−wall interaction are obtained from the work by Rahaman et al.[41] This set of force fields is known to reproduce the structures of ice nanotubes in carbon nanotubes and their melting temperatures which are obtained in the MD simulations with a rigid-body model.[42−44] A periodic boundary condition is applied in all directions; the axial direction (z-axis) of the carbon nanotube is smoothly connected, and a vacuum region outside the nanotube is sufficiently large that the self-interaction between the water-filled carbon nanotube and its images is absent. The trajectories are generated by the velocity Verlet method with a time step of 0.1 fs. The temperature is controlled using the Nosé—Hoover thermostat.

The number of confined oxygen and hydrogen atoms is 200 and 400, respectively. Here, the axial length l of the carbon nanotube is a control parameter while the axial pressure P_{zz} is obtained at each length: l is varied from 131.5 Å (consisting of 1200 carbon atoms) to 198.25 Å (1800 atoms), taking the periodicity of the carbon nanotube into account. For each condition, water molecules are randomly inserted into the carbon nanotube. The initial conformation is energy-minimized using the conjugate gradient algorithm, followed by a 10 ps equilibration MD run in the canonical ensemble (NVT). A subsequent 100 ps NVT-MD simulation is carried out for analysis.

ASSOCIATED CONTENT

Supporting Information

The Supporting Information is available free of charge at https://pubs.acs.org/doi/10.1021/acsnano.3c07084.

Movie S1: Two distinct dynamic behaviors of the hydrogen-bond networks of the $(4, 0)_3$ plastic and hydrogen-ordered ice nanotubes (MP4)

(Figure S1) Molecular structure of liquid water molecules; (Figure S2) model dependency analysis; (Figure S3) TIP4P model isothermal transformation, showing consistency with results for ReaxFF model (Figure 1c); (Figure S4) potential energy and volume contributions to enthalpy (PDF)

AUTHOR INFORMATION

Corresponding Authors

Kenji Mochizuki − *Department of Chemistry, Zhejiang University, Hangzhou 310028, People's Republic of China;* orcid.org/0000-0002-8947-9980; Email: kenji_mochizuki@zju.edu.cn

Kenichiro Koga − *Department of Chemistry and Research Institute for Interdisciplinary Science, Okayama University, Okayama 700-8530, Japan;* orcid.org/0000-0002-1153-5831; Email: koga@okayama-u.ac.jp

Author

Yuji Adachi − *Graduate School of Natural Sciences, Okayama University, Okayama 700-8530, Japan; MEC Company Ltd., Hyogo 660-0822, Japan*

Complete contact information is available at: https://pubs.acs.org/doi/10.1021/acsnano.3c07084

Notes

The authors declare no competing financial interest.

ACKNOWLEDGMENTS

We thank Mr. Xuan Zhang for making the movie. This work was supported by National Natural Science Foundation of China (Grant Nos. 22273083 and 22250610195), the Start-up Foundation for Hundred-Talent Program of Zhejiang University, and JSPS KAKENHI (Grant Nos. 18KK0151 and 20H02696).

REFERENCES

(1) Petrenko, V.; Whitworth, R. *Physics of Ice*; Oxford University Press: Oxford, U.K., 1999.

(2) Salzmann, C. G. Advances in the experimental exploration of water's phase diagram. *J. Chem. Phys.* **2019**, *150*, 060901.

(3) Millot, M.; Coppari, F.; Rygg, J. R.; Correa Barrios, A.; Hamel, S.; Swift, D. C.; Eggert, J. H. Nanosecond X-ray diffraction of shock-compressed superionic water ice. *Nature* **2019**, *569*, 251−255.

(4) Gasser, T. M.; Thoeny, A. V.; Fortes, A. D.; Loerting, T. Structural characterization of ice XIX as the second polymorph related to ice VI. *Nat. Commun.* **2021**, *12*, 1128.

(5) Yamane, R.; Komatsu, K.; Gouchi, J.; Uwatoko, Y.; Machida, S.; Hattori, T.; Ito, H.; Kagi, H. Experimental evidence for the existence of a second partially-ordered phase of ice VI. *Nat. Commun.* **2021**, *12*, 1129.

(6) Koga, K.; Zeng, X. C.; Tanaka, H. Freezing of confined water: A bilayer ice phase in hydrophobic nanopores. *Phys. Rev. Lett.* **1997**, *79*, 5262−5265.

(7) Koga, K.; Tanaka, H.; Zeng, X. C. First-order transition in conÆned water between high-density liquid and low-density amorphous phases. *Nature* **2000**, *408*, 564−567.
(8) Koga, K.; Gao, G. T.; Tanaka, H.; Zeng, X. C. Formation of ordered ice nanotubes inside carbon nanotubes. *Nature* **2001**, *412*, 802−805.
(9) Kapil, V.; Schran, C.; Zen, A.; Chen, J.; Pickard, C. J.; Michaelides, A. The first-principles phase diagram of monolayer nanoconfined water. *Nature* **2022**, *609*, 512−516.
(10) Bai, J.; Wang, J.; Zeng, X. C. Multiwalled ice helixes and ice nanotubes. *Proc. Natl. Acad. Sci. U.S.A.* **2006**, *103*, 19664−19667.
(11) Takaiwa, D.; Hatano, I.; Koga, K.; Tanaka, H. Phase diagram of water in carbon nanotubes. *Proc. Natl. Acad. Sci. U.S.A.* **2008**, *105*, 39−43.
(12) Maniwa, Y.; Kataura, H.; Abe, M.; Suzuki, S.; Achiba, Y.; Kira, H.; Matsuda, K. Phase Transition in Confined Water Inside Carbon Nanotubes. *J. Phys. Soc. Jpn.* **2002**, *71*, 2863−2866.
(13) Chin, H.-T.; Klimes, J.; Hu, I.-F.; Chen, D.-R.; Nguyen, H.-T.; Chen, T.-W.; Ma, S.-W.; Hofmann, M.; Liang, C.-T.; Hsieh, Y.-P. Ferroelectric 2D ice under graphene confinement. *Nat. Commun.* **2021**, *12*, 6291.
(14) Algara-Siller, G.; Lehtinen, O.; Wang, F. C.; Nair, R. R.; Kaiser, U.; Wu, H. A.; Geim, A. K.; Grigorieva, I. V. Square ice in graphene nanocapillaries. *Nature* **2015**, *519*, 443−445.
(15) Ma, R.; Cao, D.; Zhu, C.; Tian, Y.; Peng, J.; Guo, J.; Chen, J.; Li, X.-Z.; Francisco, J. S.; Zeng, X. C.; Xu, L.-M.; Wang, E.-G.; Jiang, Y. Atomic imaging of the edge structure and growth of a two-dimensional hexagonal ice. *Nature* **2020**, *577*, 60−63.
(16) Koga, K.; Tanaka, H. Close-packed structures and phase diagram of soft spheres in cylindrical pores. *J. Chem. Phys.* **2006**, *124*, 131103.
(17) Takii, Y.; Koga, K.; Tanaka, H. A plastic phase of water from computer simulation. *J. Chem. Phys.* **2008**, *128*, 204501.
(18) Aragones, J. L.; Vega, C. Plastic crystal phases of simple water models. *J. Chem. Phys.* **2009**, *130*, 244504.
(19) Adachi, Y.; Koga, K. Structure and phase behavior of high-density ice from molecular-dynamics simulations with the ReaxFF potential. *J. Chem. Phys.* **2020**, *153*, 114501.
(20) Jorgensen, W. L.; Chandrasekhar, J.; Madura, J. D.; Impey, R. W.; Klein, M. L. Comparison of simple potential functions for simulating liquid water. *J. Chem. Phys.* **1983**, *79*, 926−935.
(21) van Duin, C. T. A.; Dasgupta, S.; Lorant, F.; Goddard, A. William ReaxFF: A Reactive Force Field for Hydrocarbons. *J. Phys. Chem. A* **2001**, *105*, 9396−9409.
(22) Pickett, G. T.; Gross, M.; Okuyama, H. Spontaneous chirality in simple systems. *Phys. Rev. Lett.* **2000**, *85*, 3652−3655.
(23) Koga, K.; Tanaka, H. Close-packed structures and phase diagram of soft spheres in cylindrical pores. *J. Chem. Phys.* **2006**, *124*, 131103.
(24) Mochizuki, K.; Koga, K. Solid−liquid critical behavior of a cylindrically confined Lennard-Jones fluid. *Phys. Chem. Chem. Phys.* **2015**, *17*, 18437−18442.
(25) Aragones, J. L.; Conde, M. M.; Noya, E. G.; Vega, C. The phase diagram of water at high pressures as obtained by computer simulations of the TIP4P/2005 model: the appearance of a plastic crystal phase. *Phys. Chem. Chem. Phys.* **2009**, *11*, 543−555.
(26) Mochizuki, K.; Himoto, K.; Matsumoto, M. Diversity of transition pathways in the course of crystallization into ice VII. *Phys. Chem. Chem. Phys.* **2014**, *16*, 16419−16425.
(27) Yagasaki, T.; Matsumoto, M.; Tanaka, H. Phase Diagrams of TIP4P/2005, SPC/E, and TIP5P Water at High Pressure. *J. Phys. Chem. B* **2018**, *122*, 7718−7725.
(28) Henao, A.; Salazar-Rios, J. M.; Guardia, E.; Pardo, L. C. Structure and dynamics of water plastic crystals from computer simulations. *J. Chem. Phys.* **2021**, *154*, 104501.
(29) Skarmoutsos, I.; Mossa, S.; Guardia, E. The effect of polymorphism on the structural, dynamic and dielectric properties of plastic crystal water: A molecular dynamics simulation perspective. *J. Chem. Phys.* **2019**, *150*, 124506.
(30) Prasad, D.; Mitra, N. High-temperature and high-pressure plastic phase of ice at the boundary of liquid water and ice VII. *Proc. R. Soc. A* **2022**, *478*, 20210958.
(31) Hernandez, J.-A.; Caracas, R. Proton dynamics and the phase diagram of dense water ice. *J. Chem. Phys.* **2018**, *148*, 214501.
(32) Mochizuki, K.; Koga, K. Solid-liquid critical behavior of water in nanopores. *Proc. Natl. Acad. Sci. U.S.A.* **2015**, *112*, 8221−8226.
(33) Luo, C.; Fa, W.; Zhou, J.; Dong, J.; Zeng, X. C. Ferroelectric Ordering in Ice Nanotubes Confined in Carbon Nanotubes. *Nano Lett.* **2008**, *8*, 2607−2612.
(34) Torres-Dias, A. C.; Cambré, S.; Wenseleers, W.; Machon, D.; San-Miguel, A. Chirality-dependent mechanical response of empty and water-filled single-wall carbon nanotubes at high pressure. *Carbon* **2015**, *95*, 442−451.
(35) Prakapenka, V. B.; Holtgrewe, N.; Lobanov, S. S.; Goncharov, A. F. Structure and properties of two superionic ice phases. *Nat. Phys.* **2021**, *17*, 1233−1238.
(36) Corsetti, F.; Zubeltzu, J.; Artacho, E. Enhanced Configurational Entropy in High-Density Nanoconfined Bilayer Ice. *Phys. Rev. Lett.* **2016**, *116*, 085901.
(37) Chen, J.; Schusteritsch, G.; Pickard, C. J.; Salzmann, C. G.; Michaelides, A. Double-layer ice from first principles. *Phys. Rev. B Condens. Matter* **2017**, *95*, 094121.
(38) Kyakuno, H.; Matsuda, K.; Yahiro, H.; Inami, Y.; Fukuoka, T.; Miyata, Y.; Yanagi, K.; Maniwa, Y.; Kataura, H.; Saito, T.; Yumura, M.; Iijima, S. Confined water inside single-walled carbon nanotubes: global phase diagram and effect of finite length. *J. Chem. Phys.* **2011**, *134*, 244501.
(39) Plimpton, S. Fast Parallel Algorithms for Short-Range Molecular Dynamics. *J. Comput. Phys.* **1995**, *117*, 1−19.
(40) Fogarty, J. C.; Aktulga, H. M.; Grama, A. Y.; van Duin, A. C. T.; Pandit, S. A. A reactive molecular dynamics simulation of the silica-water interface. *J. Chem. Phys.* **2010**, *132*, 174704.
(41) Rahaman, O.; van Duin, A. C. T.; Goddard, W. A.; Doren, D. J. Development of a ReaxFF Reactive Force Field for Glycine and Application to Solvent Effect and Tautomerization. *J. Phys. Chem. B* **2011**, *115*, 249−261.
(42) Sobrino Fernandez Mario, M.; Neek-Amal, M.; Peeters, F. M. AA-stacked bilayer square ice between graphene layers. *Phys. Rev. B* **2015**, *92*, 245428.
(43) Satarifard, V.; Mousaei, M.; Hadadi, F.; Dix, J.; Sobrino Fernandez, M.; Carbone, P.; Beheshtian, J.; Peeters, F. M.; Neek-Amal, M. Reversible structural transition in nanodconfined ice. *Phys. Rev. B* **2017**, *95*, 064105.
(44) Raju, M.; van Duin, A.; Ihme, M. Phase transitions of ordered ice in graphene nanocapillaries and carbon nanotubes. *Sci. Rep.* **2018**, *8*, 3851.

https://doi.org/10.1021/acsnano.3c07084
ACS Nano 2024, 18, 347−354